RMetS
Royal Meteorological Society

The link between eddy-driven jet variability and weather regimes in the North Atlantic-European sector

Erica Madonna,[a,b]* Camille Li,[a,b] Christian M. Grams[c,†] and Tim Woollings[d]

[a]*Geophysical Institute, University of Bergen, Norway*
[b]*Bjerknes Centre for Climate Research, Bergen, Norway*
[c]*Institute for Atmospheric and Climate Science, ETH Zurich, Switzerland*
[d]*Atmospheric, Oceanic and Planetary Physics, Department of Physics, University of Oxford, UK*

*Correspondence to: E. Madonna, Geophysical Institute, University of Bergen, PO Box 7803, NO-5020 Bergen, Norway. E-mail: erica.madonna@uib.no

This study reconciles two perspectives on wintertime atmospheric variability in the North Atlantic–European sector: the zonal-mean framework comprising three preferred locations of the eddy-driven jet (southern, central, northern), and the weather regime framework comprising four classical North Atlantic-European regimes (Atlantic ridge AR, zonal ZO, European/Scandinavian blocking BL, Greenland anticyclone GA). A *k*-means clustering algorithm is used to characterize the two-dimensional variability of the eddy-driven jet stream, defined by the lower tropospheric zonal wind in the ERA-Interim reanalysis. The first three clusters capture the central jet and northern jet, along with a new mixed-jet configuration; a fourth cluster is needed to recover the southern jet. The mixed cluster represents a split or strongly tilted jet, neither of which is well described in the zonal-mean framework, and has a persistence of about one week, similar to the other clusters. Connections between the preferred jet locations and weather regimes are corroborated – southern to GA, central to ZO, and northern to AR. In addition, the new mixed cluster is found to be linked to European/Scandinavian blocking, whose relation to the eddy-driven jet was previously unclear.

Key Words: eddy-driven jet; weather regimes; North Atlantic atmospheric variability; blocking; NAO

Received 9 June 2017; Revised 17 August 2017; Accepted 30 August 2017; Published online in Wiley Online Library

1. Introduction

Jet streams are bands of strong westerly winds in the extratropics and a key feature of the atmospheric general circulation. They exhibit large variability over a range of timescales, and influence regional weather and climate. Jet streams are generated by two mechanisms: angular momentum transport in the thermally direct Hadley circulation creates a shallow subtropical jet aloft (Schneider, 1977; Held and Hou, 1980), while eddy momentum flux convergence from transient eddies creates a deep barotropic eddy-driven jet in midlatitudes (Held, 1975; Rhines, 1975; Panetta, 1993). Despite the different formation mechanisms, the two types of jet are not always clearly separated. If the zone of strongest baroclinicity occurs near the latitude of the subtropical jet, the two jets can merge; if the subtropical jet is weak and forms at lower latitudes, the two jets can be well separated (Lee and Kim, 2003).

The North Atlantic sector exhibits two separated jets in its wintertime climatology, with the poleward jet being primarily eddy-driven (Lorenz and Hartmann, 2003; Eichelberger and Hartmann, 2007; Li and Wettstein, 2012). The leading pattern of variability of the eddy-driven jet is a latitudinal shifting that describes 30–40% of the monthly variance (Eichelberger and Hartmann, 2007; Athanasiadis *et al.*, 2010). This shifting pattern is related to the leading pattern of North Atlantic climate variability (Thompson *et al.*, 2003; Vallis and Gerber, 2008), the North Atlantic Oscillation (NAO; Wallace and Gutzler, 1981; Hurrell, 1995). During the positive phase of the NAO (i.e. strengthening of the Icelandic low– Azores high dipole), the eddy-driven jet is more tilted and lies further polewards; during the negative phase, the jet is more zonal and lies further equatorwards (e.g. Wanner *et al.*, 2001). This characterization is useful for describing general climate relationships, but does not account for the substantial intraseasonal to interannual jet variability that determines much of the weather in the North Atlantic–European sector.

In an effort to improve our description of North Atlantic jet variability, Woollings *et al.* (2010) found that the winter

†Now at Institute of Meteorology and Climate Research (IMK-TRO), Karlsruhe Institute of Technology, Postfach 3640, 76021 Karlsruhe, Germany.

eddy-driven jet has three preferred latitudes. They linked the southern jet location to the negative NAO phase, and the central and northern jet locations to the positive and negative phases, respectively, of the East Atlantic (EA) pattern, the second most important pattern of North Atlantic climate variability. The positive NAO phase is not represented by one of these preferred locations, although the central and northern locations both project weakly onto the NAO. The central jet was also described as an undisturbed state whose location is close to the climatological jet latitude.

An alternative view of climate variability to that provided by jet variability is that of weather regimes. Starting from the concept of Grosswetterlagen in the 1940s (Baur *et al.,* 1944; Namias, 1953), weather regimes were developed as a way to categorize observed variations in geopotential height into recurrent, quasi-stationary patterns persisting beyond the life cycle of individual weather disturbances (Reinhold and Pierrehumbert, 1982; Vautard, 1990). In the North Atlantic–European sector, most studies identify four wintertime weather regimes (Vautard, 1990; Michelangeli *et al.,* 1995; Cassou, 2008; Dawson *et al.,* 2012; Hannachi *et al.,* 2017) which are closely related to atmospheric blocking: a Greenland anticyclone regime when blocking occurs mainly over Greenland (resembling the negative phase of the NAO); a zonal regime with very little blocking (resembling the positive phase of the NAO); an Atlantic ridge regime with blocking mainly offshore of the Iberian peninsula (also called Iberian wave breaking (Davini *et al.,* 2014) or southwest European blocking (Woollings *et al.,* 2010)); and a Scandinavian blocking regime with blocking mainly over the European continent and Scandinavia.

The jet location view and weather regime view are clearly related, but there is some mismatch that deserves further exploration. We expect weather regimes to be associated with variations in the eddy-driven jet because the position and strength of the jet are related to the position and strength of gradients in the geopotential height field. Moreover, flow regimes appear to have characteristic patterns of Rossby wave breaking (Benedict *et al.,* 2004; Michel and Rivière, 2011). Anticyclonic wave breaking on the equatorward flank of the jet acts to push the jet polewards, while cyclonic wave breaking on its poleward flank pushes the jet equatorwards (Thorncroft *et al.,* 1993; Rivière and Orlanski, 2007; Vallis and Gerber, 2008). While the first three North Atlantic–European weather regimes (Greenland anticyclone, zonal, Atlantic ridge) do appear to be linked to the jet latitude (southern, central, northern), the fourth regime with blocking over the European continent and Scandinavia is somewhat puzzling. Woollings *et al.* (2010) suggest that European/Scandinavian blocking is in fact decoupled from jet location. Using a different blocking index, Davini *et al.* (2014) argue that it occurs preferentially with northern jets, although it is also possible with southern jets. Other approaches link European/Scandinavian blocking to an eastward shifted variant of the negative NAO (Luo *et al.,* 2014), suggesting some relationship to southern jets.

This study aims to unify the jet and weather regime perspectives by accounting for more complex jet structures which vary on synoptic timescales. Specifically, we are interested in the following questions: (1) Are there any common jet structures that do not fit within the 'three preferred jet locations' framework? (2) Can we reconcile the three preferred jet locations with the four classical weather regimes (in particular, European/Scandinavian blocking)?

The paper is structured as follows: data and methods are explained in section 2; a motivating case-study for considering more complex jet structures is presented in section 3; a two-dimensional cluster analysis of the zonal wind is presented in section 4; and these results are compared to the classical weather regimes in section 5. Section 6 provides some discussion and concluding remarks are presented in section 7.

2. Method

The dataset used in this study is the ERA-Interim reanalysis (Dee *et al.,* 2011) from the European Centre for Medium-Range Weather Forecasts (ECMWF) with a horizontal grid spacing of 0.5° and a vertical spacing of 50 hPa. We focus on the winter season December–January–February (DJF) from 1979 to 2014, and the North Atlantic–European sector. Daily means of the following variables are used: geopotential height at 500 hPa (*Z500*), mean sea level pressure (SLP), potential vorticity (PV) on the 330 K isentrope, zonal (U) and meridional (V) wind components. For blocking and weather regimes, we additionally analyse 6-hourly PV and *Z500*.

The lower tropospheric zonal wind is used to identify the eddy-driven jet stream. The effect of eddies on the mean flow is to decrease the vertical shear and to accelerate the barotropic westerly flow, particularly at lower levels (e.g. Hoskins *et al.,* 1983). The upper-level wind might also be partly thermally driven, even in the North Atlantic sector (Li and Wettstein, 2012). Thus, the lower-level wind is considered best for diagnosing the variability of the eddy-driven jet (Woollings *et al.,* 2010). We use daily values of the zonal wind (U) and apply a 10-day low-pass filter to reduce the influence of short-lived, localized and strong wind features associated, for example, with individual synoptic systems. The filter is a top-hat, the standard low-pass filter implemented in the Climate Data Operators package (CDO, 2015), with a passband between 0 and 1/10 day^{-1}, and is applied to daily averages for the entire ERA-Interim period before selecting the winter season. The 'lower tropospheric' zonal wind (U^*_{low}) is then obtained by averaging the low-pass filtered wind between 900 and 700 hPa.

2.1. Jet latitude index

We calculate the jet latitude index (JLI) in a way similar to Woollings *et al.* (2010). U^*_{low} is zonally averaged over the North Atlantic sector (60–0°W longitude, 15–75°N latitude), and the JLI is defined as the latitude where the maximum is found. Here, we use the absolute latitude instead of the latitude anomaly. Because we focus on the winter season, the seasonal cycle has not been removed. The JLI from ERA-Interim is nearly identical to that calculated from ERA-40 by Woollings *et al.* (2010). It exhibits three clear maxima, as derived from kernel estimation probability density functions (Figure 1 in Woollings *et al.* (2010) and grey dashed line in Figure 4). The three preferred jet locations are at approximatively 36°N (southern jet S), 45°N (central jet C) and 58°N (northern jet N).

2.2. Cluster analysis

Cluster analysis techniques have been widely used to identify recurrent and quasi-stationary states of the large-scale atmospheric circulation, also known as weather regimes (e.g. Vautard, 1990; Cheng and Wallace, 1993; Michelangeli *et al.,* 1995; Michel and Rivière, 2011). They have also been applied to one-dimensional jet profiles (Frame *et al.,* 2011) and atmospheric indices (Hannachi *et al.,* 2012). The two common clustering approaches are hierarchical methods (e.g. Ward's method) and partitioning methods (e.g. k-means). The main advantage of hierarchical methods is that the number of clusters does not have to be specified *a priori*, but these methods are computationally expensive and less flexible than partitioning methods. Partitioning methods, while computationally efficient, require an *a priori* decision on the number of clusters k. Depending on the research focus, clustering can be performed on various fields (e.g. mid-tropospheric geopotential height, lower-tropospheric zonal wind) pre-processed in various ways (e.g. filtered to separate timescales or to reduce data dimensionality).

In this study we use k-means clustering similar to Michelangeli *et al.* (1995). Empirical orthogonal function (EOF) analysis is applied to the area-weighted U^*_{low} anomalies in the North Atlantic

sector (60–0°W longitude, 15–75°N latitude) and five EOFs (80% of the sectoral wintertime variance) are retained. Retaining four to six EOFs (76–83% of the variance) produces essentially the same results; with more than seven EOFs retained, the cluster analysis begins to yield structures with undesirable noise (not shown). A *k*-means clustering algorithm then assigns each observation (daily U^*_{low} anomaly) to one of *k* clusters, where *k* (the number of clusters) is chosen *a priori*. Specifically, the algorithm identifies the *k* cluster centroids that minimize the within-cluster spread, defined as the sum of the squared Euclidean distance of each observation from its cluster centroid. The algorithm is applied ten times to the same dataset to ensure that the clusters are 'stable', i.e. the resulting centroids are identical for different random starting points (seeds).

To compare results for different choices of *k*, we produce zonal wind composites for each cluster and compute pattern correlations (*Rp*) between clusters. The pattern correlation is given by the area-weighted spatial covariance between two composites, *a* and *b*, divided by the product of their area-weighted standard deviations:

$$Rp = \frac{cov(a,b)}{\sigma(a)\cdot\sigma(b)}. \tag{1}$$

The covariance is defined as

$$cov(a,b) = \frac{1}{\sum_{j=1}^{M} cos(\phi_j)} \frac{1}{NM} \sum_{i=1}^{N}\sum_{j=1}^{M} cos(\phi_j)\cdot(a_{ij}-\overline{a})(b_{ij}-\overline{b}) \tag{2}$$

and the standard deviation as

$$\sigma(a) = \sqrt{\frac{1}{\sum_{j=1}^{M} cos(\phi_j)} \frac{1}{NM} \sum_{i=1}^{N}\sum_{j=1}^{M} cos(\phi_j)\cdot(a_{ij}-\overline{a})^2}, \tag{3}$$

where $\overline{a}, \overline{b}$ are North Atlantic sectoral means of the composites; *N*, *M* are the number of longitude, latitude points; and ϕ is the latitude. Values of *Rp* close to one indicate that the composites are similar.

2.3. Weather regimes

Weather regimes can be identified using various methods, including pattern correlation or cluster analysis, applied to various meteorological fields (e.g. Molteni *et al.,* 1990; Vautard, 1990; Cheng and Wallace, 1993; Kimoto and Ghil, 1993; Michelangeli *et al.,* 1995). For this study, weather regimes are defined using 6-hourly anomalies of *Z500* (with respect to the 1979–2014 mean of 6-hourly values, smoothed by a 30-day running mean) that have been low-pass filtered to retain variability on timescales longer than 10 days. We focus on the DJF winter season, for which previous studies report the existence of four North Atlantic–European regimes (Vautard, 1990; Michelangeli *et al.,* 1995; Cassou, 2008; Dawson *et al.,* 2012; Ferranti *et al.,* 2015), with the exact patterns depending slightly on the definition of the season (discussion in Supplement of Cassou, 2008; Grams *et al.,* 2017). In line with other studies (e.g. Michel and Rivière, 2011; Ferranti *et al.,* 2015), *k*-means cluster analysis is performed over a larger North Atlantic–European sector extending from 80°W to 40°E and from 30 to 90°N.

The four identified weather regimes are named following the nomenclature of Vautard (1990): Atlantic ridge (AR), zonal (ZO), European/Scandinavian blocking (BL), and Greenland anticyclone (GA).

2.4. NAO and EA indices

The North Atlantic Oscillation (NAO) and East Atlantic (EA) pattern time series are the first two principal components derived from an EOF analysis of daily *Z500* anomalies (with respect to the 1979–2014 mean of daily values) over 75°W–15°E and 20–90°N. We use the same sign convention for the EA index as Woollings *et al.* (2010), such that the positive phase has a cyclonic anomaly in the mid-Atlantic. This method gives similar results to the projection of the daily *Z500* anomalies onto monthly NAO and EA patterns (Hannachi *et al.,* 2012).

2.5. Blocking

Blocking is identified based on anomalies (derived by subtracting from each 6-hourly time step the corresponding monthly climatology for the 1979–2014 period) in vertically averaged (500 to 150 hPa) PV following the method of Schwierz *et al.* (2004). A block is detected if a region exhibits a negative anomaly lower than −0.7 pvu that is quasi-stationary (spatial overlap of 70% for two consecutive 6-hourly time steps) and persistent (spatial overlap fulfilled for at least a 5-day period). We use this PV threshold which is less strict than other studies (e.g. −1.2 pvu in Pfahl *et al.,* 2015) to include weaker blocks that still characterize the different regimes as well as enhanced subtropical anticyclones at lower latitudes. The more strict threshold (−1.2 pvu) would reveal similar blocking patterns, but with an overall reduced frequency (not shown).

3. Case-studies

The JLI is overall a simple and useful way to characterize the Atlantic eddy-driven jet and its variability, as we will discuss using four example winters (1996/1997, 2004/2005, 2009/2010 and 2013/2014, Figure 1). Each of these winters exhibits coherent zonal-mean jet structures (shading) which the JLI (black line) tracks quite faithfully. The JLI hence picks out important differences from winter to winter in terms of the latitudinal position and variability of the jet. For instance, the winter of 2009/2010 was characterized by a strong and persistent negative NAO (e.g. Cattiaux *et al.,* 2010; Ouzeau *et al.,* 2011), and a southward shifted North Atlantic jet (Santos *et al.,* 2013; Harnik *et al.,* 2014). The JLI (black line, Figure 1(c)) is centred around the preferred southern location (southern horizontal dashed line, Figure 1(c)) for most of this particular winter. During other winters, the JLI indicates a persistent central (Figure 1(d)) or northern (Figure 1(b)) jet. The winter of 1996/1997, on the other hand, shows high intraseasonal variability, with the JLI visiting all three preferred latitudes (Figure 1(a)).

Closer examination of Figure 1 reveals periods when the JLI deviates somewhat from the zonal-mean wind field. During the 1996/1997 winter, there is a period of relatively constant, weak (less than 15 m s^{-1}) zonal-mean U^*_{low} when the JLI makes several large, latitudinal jumps (Figure 1(a), day 45–55). Another complication occurs when the zonal-mean U^*_{low} exhibits multiple local maxima, as for example during winter 2009/2010. Here, the JLI jumps rapidly from one maximum to the other and back again (Figure 1(c), day 55–65). In such situations, the zonal-mean perspective misses the real-world complexity of the jet, and identifying the zonal-mean jet position is not straightforward.

To better illustrate the relationship between the zonal-mean and zonally varying viewpoints, we choose four example days from the winter of 1996/1997 (grey arrows, Figure 1(a)) and examine the corresponding synoptic maps (Figure 2). On 2 December 1996, the synoptic map (Figure 2(a)) shows a clear eddy-driven jet (black contours) at a high northern latitude, in good agreement with the JLI (green line at 57.5°N). The eddy-driven jet sits at the northern flank of a region of enhanced SLP (shading) spreading across the North Atlantic, collocated with an upper level ridge (2 pvu contour on the 330K isentrope

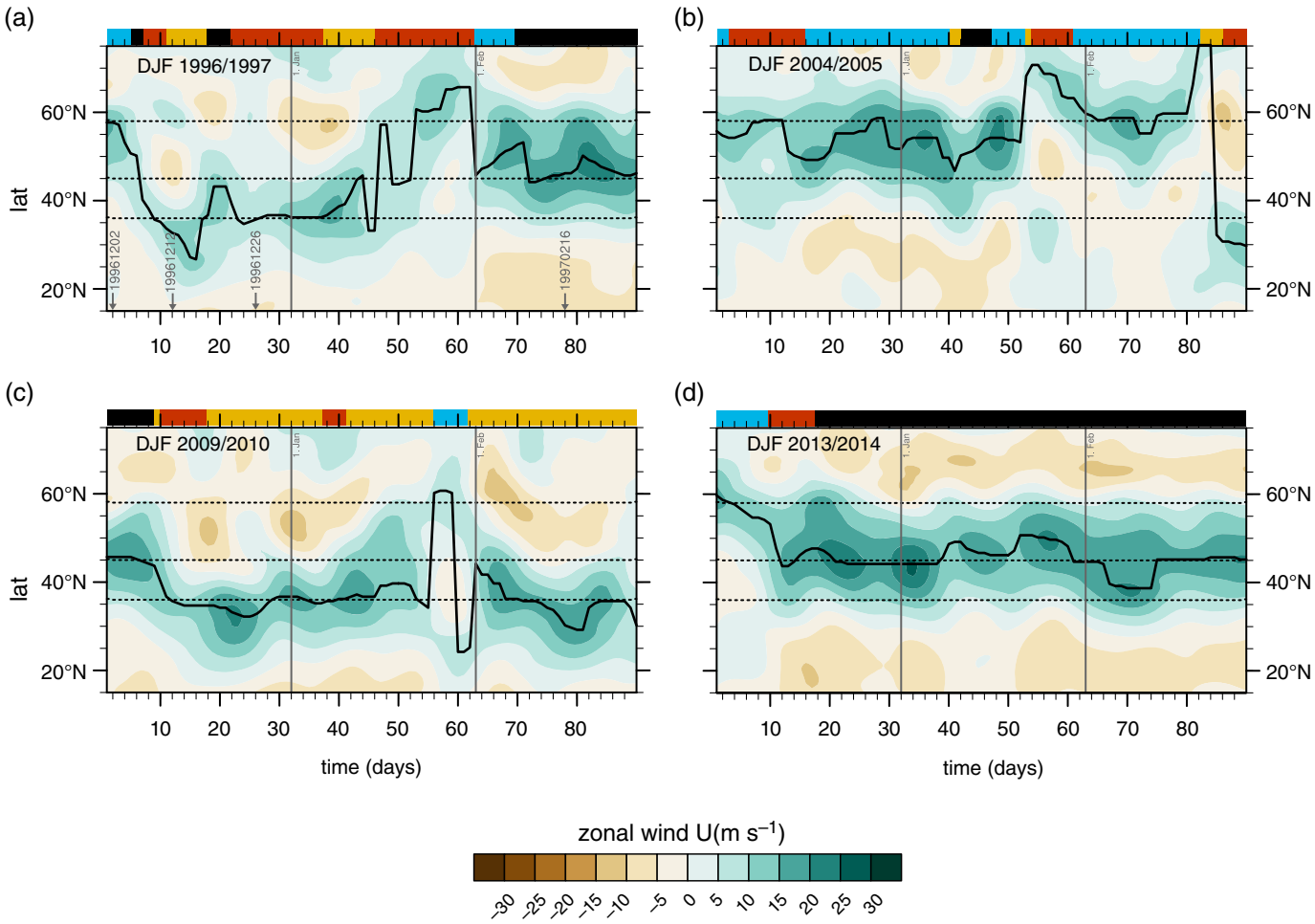

Figure 1. Time–latitude plots (starting on December 1) of the eddy-driven jet for the DJF winter seasons (a) 1996/1997, (b) 2004/2005, (c) 2009/2010 and (d) 2013/2014. Shading shows daily low-pass filtered zonal wind between 900 and 700 hPa (U^*_{low}) zonally averaged over 60–0°W. The JLI (black line) indicates the latitude of the jet using the approach of Woollings *et al.* (2010). The horizontal dashed lines show the three preferred jet locations (section 2.1). The labelled arrows in (a) denote the days shown in Figure 2. The coloured bars over each panel show which jet cluster the day belongs to (N_4 in blue, C_4 in black, M_4 in red and S_4 in orange). [Colour figure can be viewed at wileyonlinelibrary.com].

in red, indicating the dynamical tropopause). The dynamical tropopause generally follows the jet, but there is an elongated PV streamer reaching equatorward to 20°N at the western edge of the sector. On 12 December 1996 there are two maxima in the low-level wind speed in the North Atlantic sector, with a stronger, broader and tilted southern maximum which is mainly collocated with the JLI (green line at 32.5°N, Figure 2(b)). A high pressure system is found south of Greenland and a low pressure system sits offshore of the Iberian peninsula. In the northwestern part of the sector we observe upper-level cyclonic Rossby wave breaking. On 26 December 1996 (Figure 2(c)), there are three wind maxima: two strong ones (10–15 m s^{-1}) in the northern part of the domain, and a weaker (5–10 m s^{-1}) branch in the subtropics. The zonal-mean perspective (Figure 1(a)) shows weak westerlies at all latitudes, which are the result of averaging over these three maxima (Figure 2(c)). The strongest winds are in the northern maxima. However, the JLI (green line at 35.5°N) captures the southern maximum, which is weaker but extends over a larger longitudinal range. The split-jet structure is accompanied by a strong high pressure over northern Europe and Scandinavia and a pronounced upper level trough in the middle of the North Atlantic sector. Finally, the last example (16 February 1997, Figure 2(d)) shows a cyclone–anticyclone dipole in the North Atlantic and a strong jet located in the centre of the domain, in the region of the strongest pressure gradient. The JLI is detected close to the central preferred jet location.

In summary, the JLI works well for describing the eddy-driven jets in most cases, but less well when the jet deviates from a relatively zonal structure (e.g. tilted as in Figure 2(b) or split as in Figure 2(c)). Next, we consider the jet's zonally varying structure in an attempt to capture a fuller range of its variability.

4. Jet clusters

On synoptic timescales, the structure of the eddy-driven jet stream can be quite complex and therefore challenging to describe using a single index. Some alternatives exist. For example, Messori and Caballero (2015) introduced the concept of jet angle to account for tilted jets. Other methods have been developed to identify more complicated jet structures (e.g. Koch *et al.*, 2006; Schiemann *et al.*, 2009; Limbach *et al.*, 2012; Spensberger *et al.*, 2017), but these are feature-based and/or focus on upper-level jets, which are not purely eddy-driven.

Two-dimensional cluster analysis offers a way to characterize jet structures that allows for both tilted and split jets. A key question is how to determine a meaningful number of clusters k, as this value must be specified *a priori*. Since the North Atlantic eddy-driven jet stream has been shown to have three preferred latitudinal locations, it seems natural to start with $k = 3$ clusters on the lower tropospheric wind (section 2.2). Additionally, we perform the cluster analysis for larger values of k, and compare the resulting clusters. Note that, because each day must be classified into a cluster and because the transition from one cluster to another is not instantaneous, there are days that exhibit substantial similarity to more than one cluster. Such days are included in the cluster composites shown here, but the main results do not change when using only the days closest to each cluster centroid.

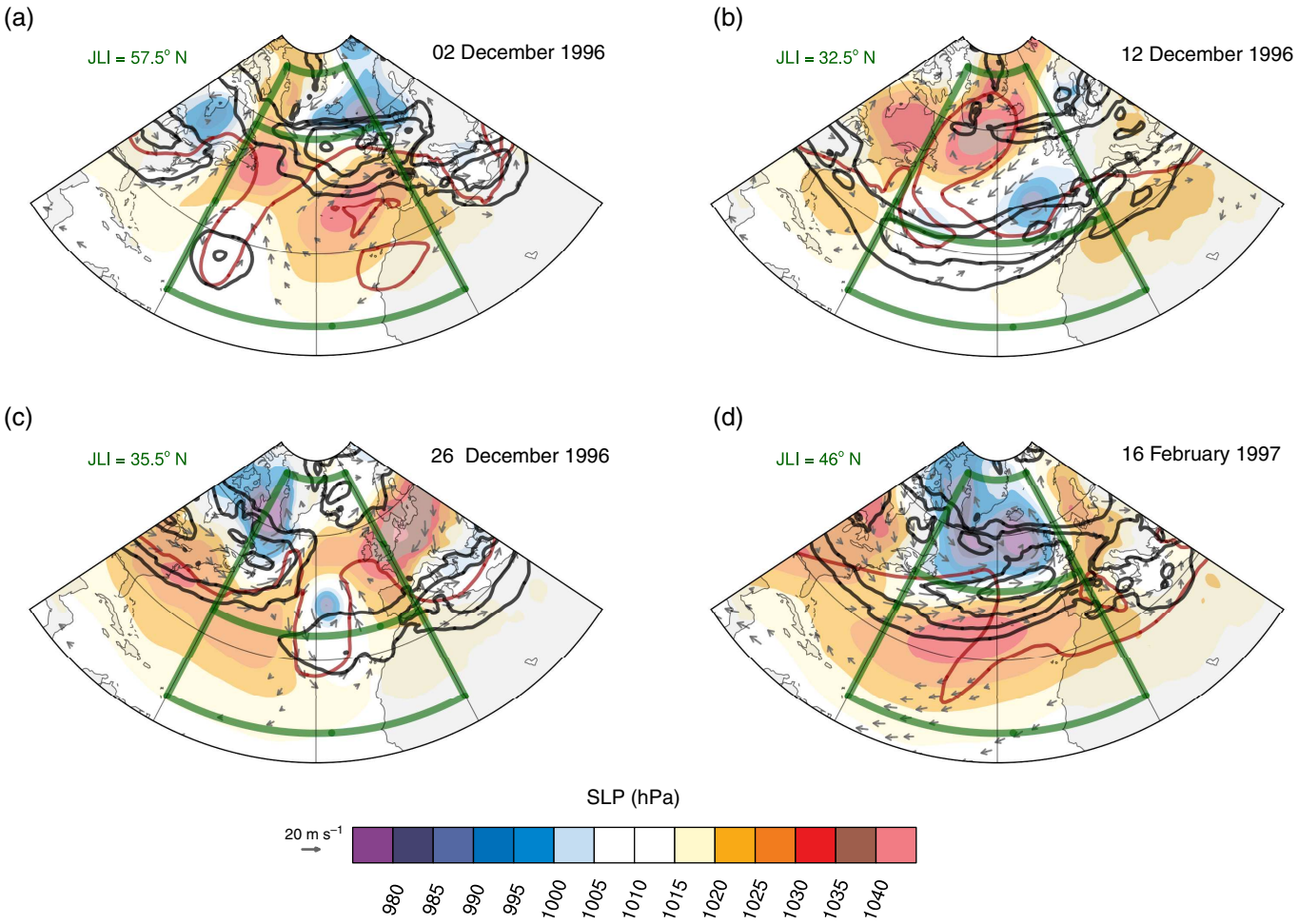

Figure 2. Synoptic maps (daily means) for four different days during the 1996/1997 winter, showing the lower tropospheric wind speed U^*_{low} (black contours, 5 m s^{-1} intervals from 5 m s^{-1}), daily winds at 850 hPa (grey arrows starting from 20 m s^{-1}), sea level pressure (SLP, colour shading), and 2-pvu on the 330K isentrope (red contours). The green box shows the North Atlantic domain, and the green line shows the latitude of maximum zonal-mean U^*_{low} in the domain (i.e. the JLI, value shown at top left of each panel). The days are as indicated in the time–latitude plot of Figure 1(a): (a) 2 December 1996 (N_4 cluster), (b) 12 December 1996 (S_4 cluster), (c) 26 December 1996 (M_4 cluster), (d) 16 February 1997 (C_4 cluster). [Colour figure can be viewed at wileyonlinelibrary.com].

Surprisingly, with $k = 3$, we find counterparts for only the northern and central preferred jet locations from the JLI framework, and not the southern jet location. The first cluster, termed N_3 (N for north and 3 for $k = 3$, the number of clusters; first panel, Figure 3(a)) comprises 1061 days and exhibits a maximum in U^*_{low} (black contours) in the northern part of the domain, between 50° N and 60° N. The highest standard deviations in U^*_{low} (shading) are collocated with the wind maximum, and the standard deviation does not exceed 8 m s^{-1} (approximately 50% of the maximum wind). This resembles the wind composite for the northern jet location using the JLI (cf. Woollings *et al.*, 2010, their Figure 6). To verify, the JLI was calculated for all days in the N_3 cluster (blue line, Figure 4(a)). It has a peak between 50 and 60°N, showing that N_3 accounts for a large part of the northern peak in the climatological wintertime JLI distribution (grey dashed line, Figure 4(a)). The second cluster, C_3 (central; second panel, Figure 3(a)), comprises 1048 days and exhibits a tilted wind maximum in the centre of the domain around 40°N. For this cluster, the highest standard deviations are not collocated with the wind maximum as for N_3; rather, there is large variability on the northern and southern flanks of the maximum. The JLI for the C_3 cluster (black line, Figure 4(a)) is most often at latitudes between 40 and 50°N, similar to the preferred latitude of the central jet location, but with more occurrences of the JLI at latitudes south of 40°N which contribute to the southern peak in the climatological wintertime distribution. Finally, the third cluster (1041 days; third panel, Figure 3(a)), which we might have expected to resemble the southern jet location, does not. Instead of a wind maximum in the southern part of the domain, it has two distinct maxima in the southwestern and northeastern parts of the domain, with the highest standard deviations found between the maxima. The associated JLI (red curve, Figure 4(a)) is also curious: it covers a wide range of latitudes and with slightly higher frequencies close to both the southern and northern peaks of the wintertime climatology. Because the cluster composite shows a somewhat split jet structure with a strong tilt, we call this the 'mixed' cluster (M_3).

The missing southern jet location from the JLI framework emerges with an additional cluster ($k = 4$). The northern cluster N_4 (first column, Figure 3(b)) is similar to the N_3 cluster in terms of wind strength and variance, as well as JLI distribution (blue line, Figure 4(b)). Of the 799 days in this cluster, 772 (97%) were classified in the former northern cluster (N_3). The central cluster C_4 exhibits a more zonal jet than C_3, with reduced variability, especially on the southern flank of the jet. The JLI has a clearer peak in C_4 than C_3, centred between 40 and 50°N with almost no occurrences south of 40°N (compare black lines in Figures 4(b) and (a)). The mixed cluster M_4 is the most populated cluster (875 days) and it is similar to the M_3 cluster but with stronger maxima. The JLI (red line, Figure 4(b)), as previously with $k = 3$, covers a wide range latitudes, although the southern peak is less pronounced. Finally, in the fourth cluster, the wind composite shows the jet in the southern part of the domain, with a clear wind maximum around 35°N and enhanced variance to the north. The JLI (orange line, Figure 4(b)) is most frequently between 30 and 45°N, which accounts for a large part of the southern peak in the climatological wintertime distribution.

Introducing a fifth cluster ($k = 5$), the main change is that the mixed cluster is further refined into a tilted jet configuration T_5 along with the existing split jet M_5 (Figure 3(c)). The previously

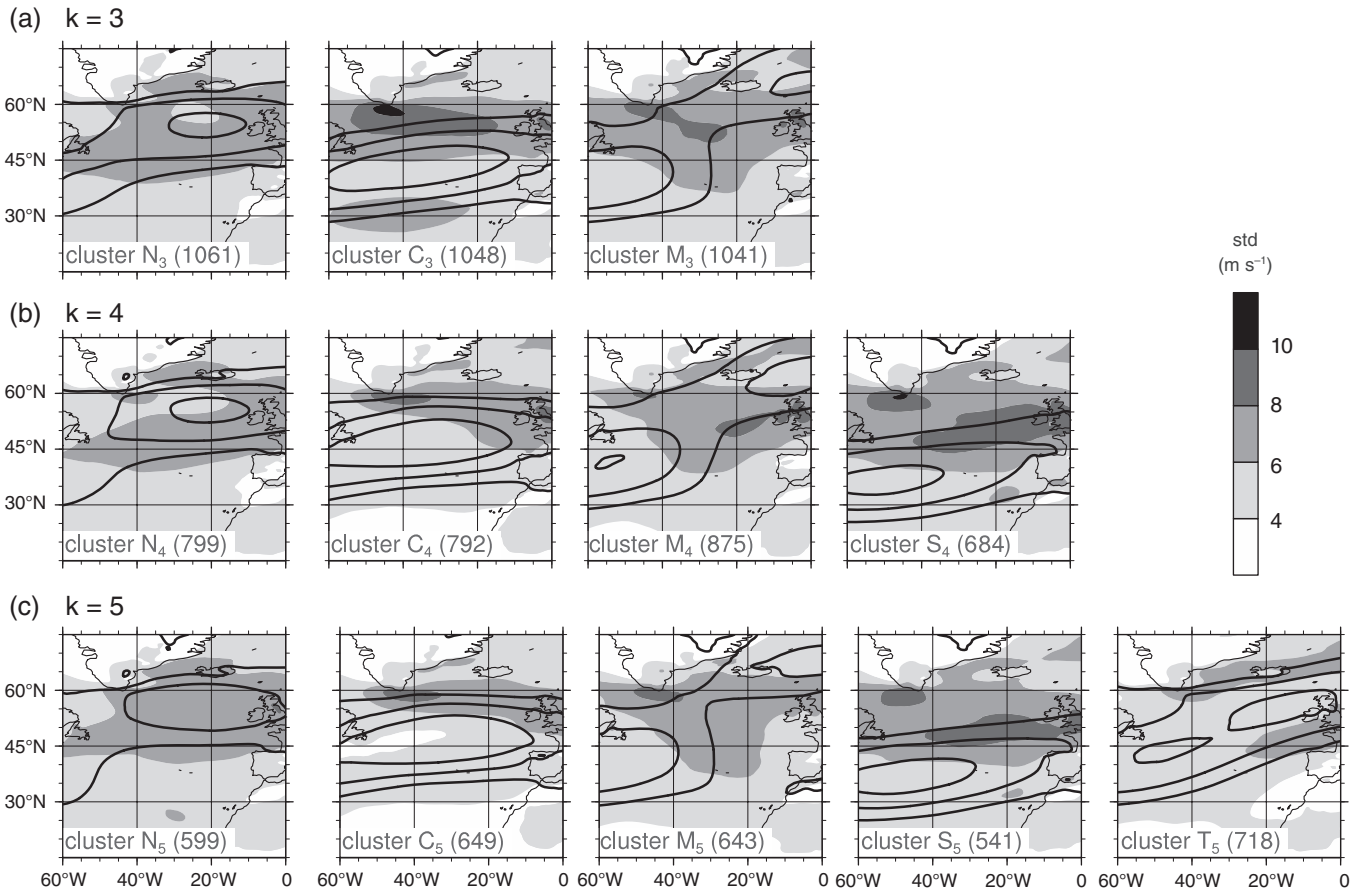

Figure 3. Composites of the eddy-driven jet during DJF winter for (a) $k=3$, (b) $k=4$ and (c) $k=5$ clustering results. Shown are the lower tropospheric wind speed U^*_{low} (contours every 5 m s^{-1}, starting at 5 m s^{-1}) together with their standard deviation (std, shading). From left to right are the northern (N_k), central (C_k), and mixed (M_k) clusters for all values of k, the southern (S_k)clusters for $k=4$ and $k=5$, and the tilted (T_k) cluster for k=5. The numbers at the bottom of each panel indicate the days in each cluster (also given in Table 1).

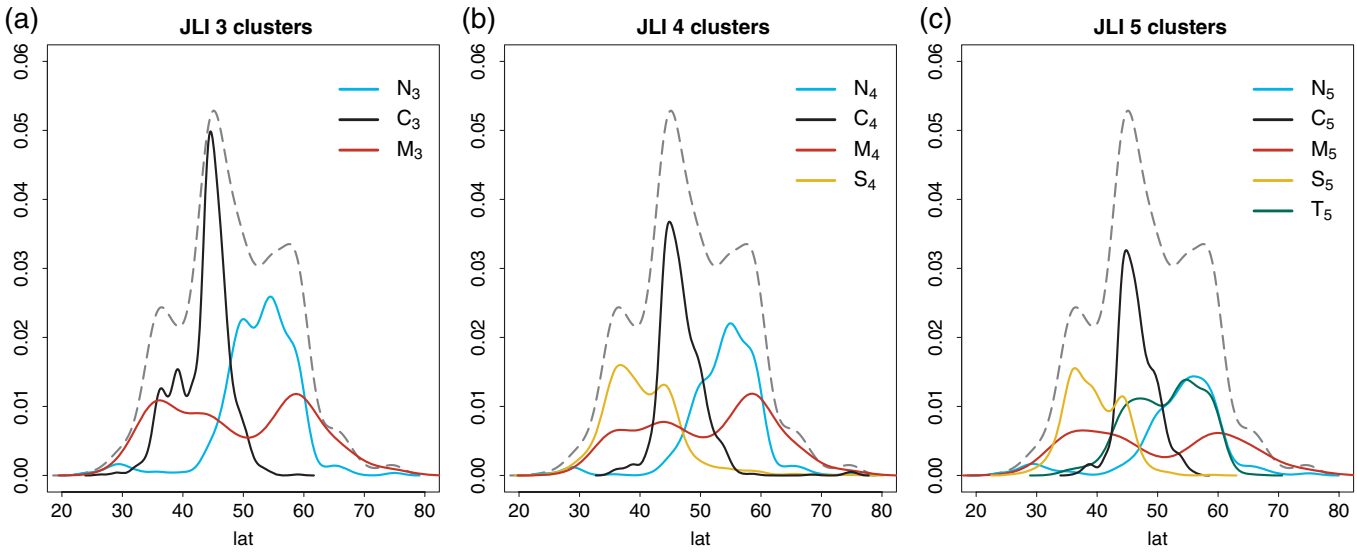

Figure 4. JLI distribution during DJF winter for (a) $k=3$, (b) $k=4$ and (c) $k=5$ clustering results, showing the probability density functions (via kernel estimations) of the daily distribution of the JLI in the North Atlantic sector. Colours indicate the cluster: northern N_k in blue, central C_k in black, mixed M_k in red, southern S_k in orange and tilted T_k in green. The probability density functions are scaled by the number of days in each cluster and the grey dashed line shows the full distribution (i.e. the ERA-Interim DJF climatology). [Colour figure can be viewed at wileyonlinelibrary.com].

identified N, C and S clusters for $k=5$ are very similar to $k=4$, as are the standard deviations of the wind composites. The new cluster T_5 includes nearly equal contributions from the former mixed M_4 (234 days) and northern N_4 (292 days) clusters, and leaves the new northern cluster N_5 with a weaker wind maximum than N_3 and N_4. The JLI for the tilted cluster (green curve, Figure 4(c)) spans the central and northern preferred jet locations.

By adding more clusters, we allow for cleaner separation between certain jet configurations, but we also end up with clusters that look more similar. This is shown in Table 1, which reports the pattern correlation (Rp) between the wind composites of various clusters for different values of k. The choice of $k=3$ seems reasonable in the light of the JLI framework, but the three clusters that emerge capture only the northern and central preferred jet locations, and not the southern. The highest pattern

Table 1. Pattern correlations Rp between clusters for $k=3$, $k=4$ and $k=5$ clustering results (N: northern, C: central, M: mixed, S: southern, T: tilted).

Cluster	N_k	C_k	M_k	S_k	T_k
N_3 (1061)	1.00				
C_3 (1048)	**0.63**	1.00			
M_3 (1041)	0.59	0.62	1.00		
N_4 (799)	1.00				
C_4 (792)	**0.72**	1.00			
M_4 (875)	0.67	0.67	1.00		
S_4 (648)	0.22	0.65	0.51	1.00	
N_5 (599)	1.00				
C_5 (649)	0.62	1.00			
M_5 (643)	0.39	0.50			
S_5 (541)	0.04	0.60	0.45	1.00	
T_5 (718)	0.84	**0.86**	0.62	0.46	1.00

Numbers in the brackets indicate the number of days belonging to each cluster. Bold numbers are the highest pattern correlation for each k.

Table 2. Persistence (days) of the $k=4$ clusters (N_4: northern, C_4: central, M_4: mixed, S_4: southern).

Cluster	Mean	Median	Maximum
N_4	7.0	6	32
C_4	6.8	5	38
M_4	7.3	6	25
S_4	8.0	6	32

correlation between any two clusters is $Rp(N_3, C_3)=0.63$. The choice of $k=4$ also seems reasonable, as there is strong evidence for the existence of four recurrent and quasi-stationary regimes in the large-scale atmospheric circulation (e.g. Vautard, 1990; Michelangeli *et al.*, 1995). Among the $k=4$ clusters, we find the three preferred jet locations, as well as the mixed cluster. The new southern cluster is quite distinct, especially from the northern cluster ($Rp(N_4, S_4)=0.22$), but the two most similar clusters become slightly more similar ($Rp(N_4, C_4)=0.72$). Adding a fifth cluster more clearly distinguishes between split jets and tilted jets. The new tilted cluster is highly correlated with both the central ($Rp(C_5, T_5)=0.86$) and northern ($Rp(N_5, C_5)=0.84$) clusters, but the similarity between all other clusters decreases.

The rest of the paper will focus on the $k=4$ results since the main goal of this study is to reconcile the jet and weather regime perspectives. There is good agreement between the $k=4$ clusters and the JLI during well-behaved winters: the 2004/2005 winter is dominated by a northern jet and the N_4 cluster (blue segments in top bar, Figure 1(b)); the 2009/2010 winter is dominated by a southern jet and the S_4 cluster (orange segments, Figure 1(c)); and the 2013/2014 winter is dominated by a central jet and the C_4 cluster (black segments, Figure 1(d)). The additional M_4 cluster helps clarify periods when the zonal-mean wind struggles to capture a more complicated, zonally varying jet structure. The 1996/1997 winter had an extremely variable jet with a substantial presence of all four clusters (Figure 1(a)). The mixed M_4 cluster (red segments) occurs mainly during periods when the zonal wind is weak (e.g. days 48–60) or more than one maximum exists (e.g. days 22–35). For M_4 days during this winter, the JLI is typically in the northern (e.g. days 50–60) or southern (e.g. days 25–30) location, a result that holds more generally for the entire ERA-Interim period as well (red line, Figure 4(b)).

A legitimate question is whether the mixed cluster is just a transition phase between the southern, central and northern clusters. If so, one might expect a considerably shorter persistence of the mixed cluster. The mean, median and maximum number of consecutive days in each cluster are shown in Table 2. The mixed cluster M_4 is as persistent as the others, refuting the transition hypothesis. A similar conclusion holds for $k=3$ or $k=5$ clusters (not shown). With a mean duration of 7.3 days, M_4 is second only to S_4, which is the most persistent state, in agreement with previous studies (e.g. Barnes *et al.*, 2010).

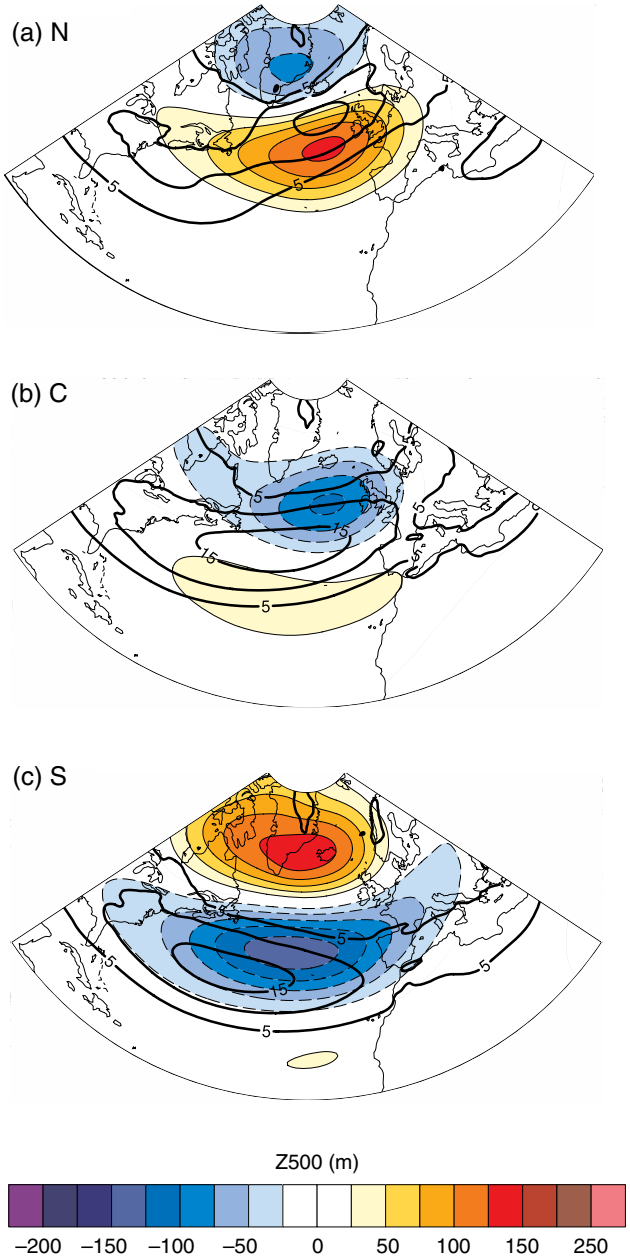

Figure 5. Circulation composites during DJF winter for the three preferred jet locations: (a) northern, (b) central and (c) southern. Composites show geopotential height anomalies (*Z500*; shading) and lower tropospheric wind speed U^*_{low} (black contours, 5 m s^{-1} intervals from 5 m s^{-1}) for all days with a JLI within 10° latitude of the corresponding preferred jet latitude, identified as the maxima of the climatological probability density function (grey dashed line) in Figure 4. The composites are similar to those in Woollings *et al.* (2010) (their Figure 4) and Hannachi *et al.* (2012) (their Figure 3). [Colour figure can be viewed at wileyonlinelibrary.com].

5. Relation to blocking and weather regimes

There remain some open questions in connecting the North Atlantic eddy-driven jet to atmospheric blocking and weather regimes, as described in the introduction. The three preferred jet locations (southern, central, northern) seem clearly linked to three of the four characteristic blocking situations (Greenland blocking, no blocking, blocking offshore of Iberian peninsula), but there is some disagreement over the nature of the jet during European/Scandinavian blocking. Woollings *et al.* (2010) concluded that it occurs for all jet locations and it is hence decoupled from the jet stream, while Davini *et al.* (2014) argued that it is mainly associated with northern jets, but also possible with southern jets. This mismatch extends to the four weather regimes because they are also related to blocking situations, with the BL regime seemingly having no clear preferred jet location. In this section, we ask how the picture changes when moving from the zonal-mean framework of three preferred jet locations

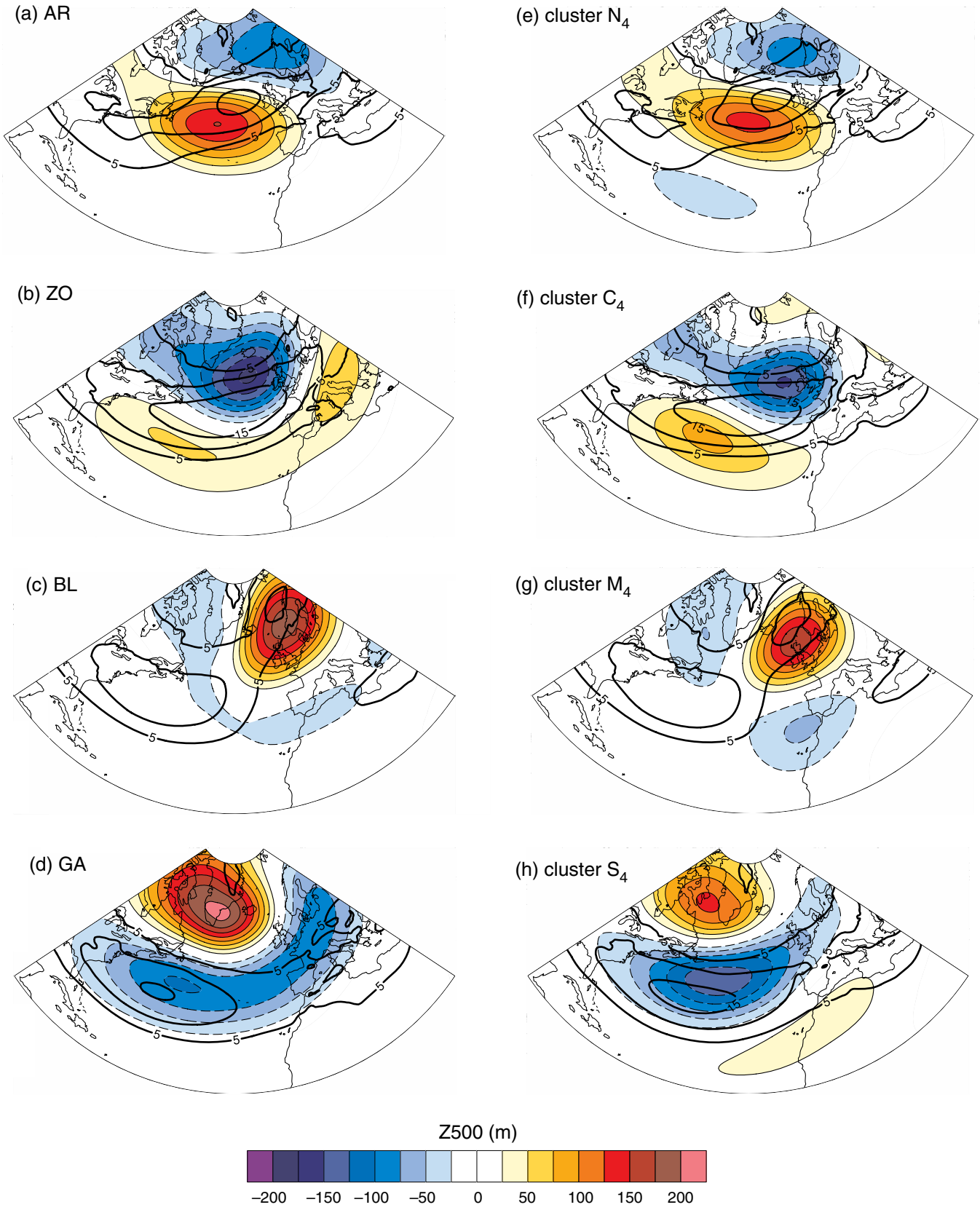

Figure 6. Circulation composites during DJF winter for (a)–(d) the four classical North Atlantic–European weather regimes and (e)–(h) $k=4$ clustering results. Composites show geopotential height anomalies (*Z500*; shading) and lower tropospheric wind speed U^*_{low} (black contours, 5 m s^{-1} intervals from 5 m s^{-1}) for days belonging to each weather regime or cluster. The four regimes are (a) Atlantic ridge (AR), (b) zonal (ZO), (c) Scandinavian blocking (BL), and (d) Greenland anticyclone (GA). The four clusters are (e) northern N_4, (f) central C_4, (g) mixed M_4, and (h) southern S_4. [Colour figure can be viewed at wileyonlinelibrary.com].

(Figure 5) to the zonally varying framework of four jet clusters (Figure 6). Not only do we find a link to the problematic BL regime and European/Scandinavian blocking, but there is also better agreement of the geopotential anomalies patterns between the remaining three weather regimes and jet clusters.

First, we compare the three patterns that correspond well across the various frameworks. Starting with the three preferred locations, the *Z500* composite for the southern jet location (shading, Figure 5(c)) resembles the negative pattern of the NAO, with an Iceland–Azores dipole and a zonally oriented eddy-driven jet (U^*_{low}, black contours). The *Z500* patterns and jet structure are very similar for both the GA regime (Figure 6(d)) and the S_4 cluster (Figure 6(h)). The northern and central jet composites (Figures 5(a) and (b)) resemble the negative and positive phases

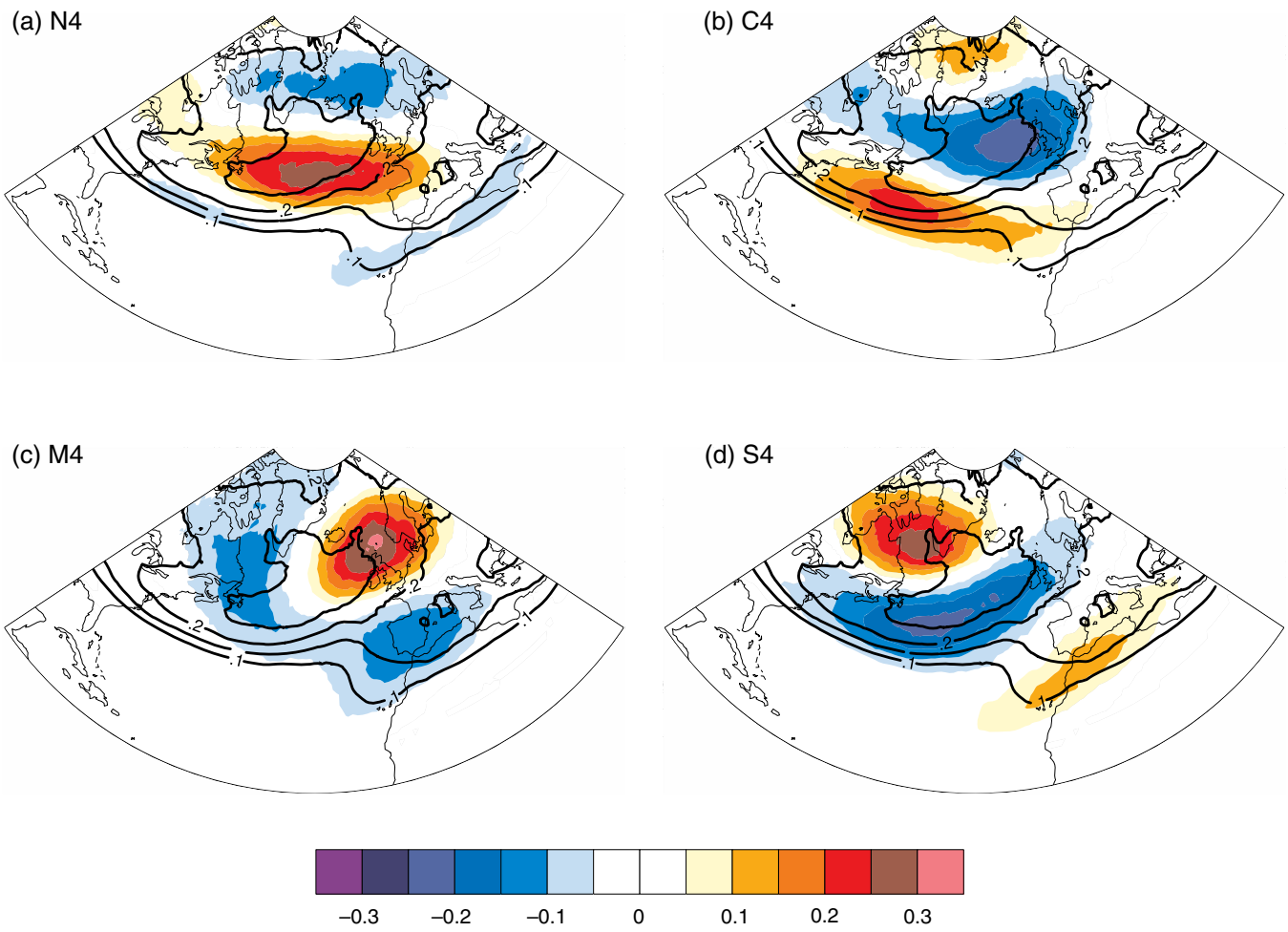

Figure 7. Blocking anomalies (shading) during DJF winter for the $k = 4$ clustering results: (a) northern N_4, (b) central C_4, (c) mixed M_4 and (d) southern S_4. The DJF blocking climatology is shown in black contours (0.05 or 5% intervals from 0.1). Blocking is based on a PV anomaly threshold of −0.7 pvu following the approach of Schwierz *et al.* (2004) (details in section 2.5). [Colour figure can be viewed at wileyonlinelibrary.com].

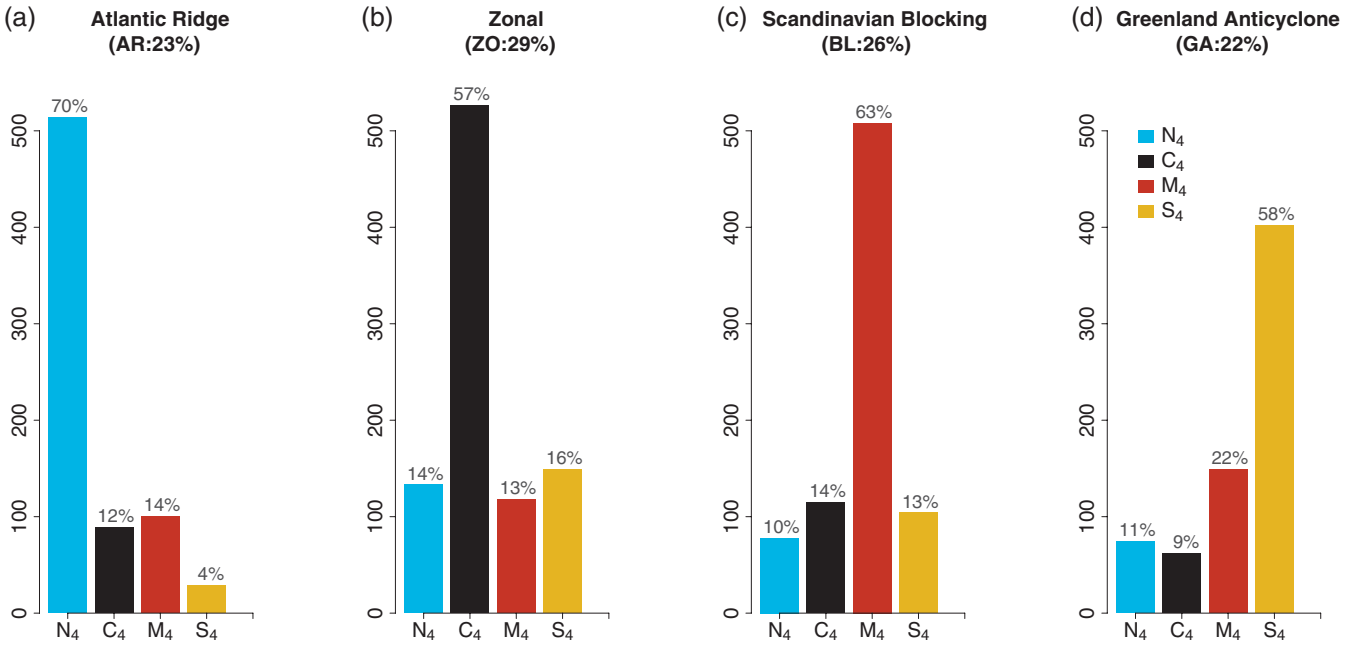

Figure 8. Partitioning of North Atlantic-European weather regimes by jet cluster for the four regimes: (a) Atlantic ridge, (b) zonal, (c) Scandinavian blocking, and (d) Greenland anticyclone. Colours indicate the number of days belonging to each cluster: northern N_4 (blue), central C_4 (black), mixed M_4 (red), and southern S_4 (orange). The occurrence of each weather regime (in %) is shown at the top of each panel. The frequency of each cluster within the regimes (in %) is shown at the top of the bars, and add up to 100% in each panel. [Colour figure can be viewed at wileyonlinelibrary.com].

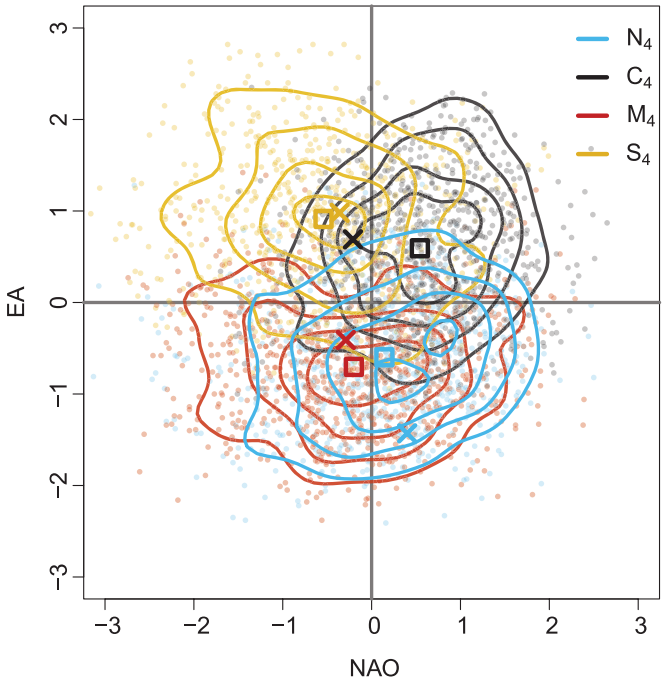

Figure 9. Distribution of jet clusters in NAO–EA space. The NAO and EA indices are the first two normalized PCs of daily *Z500*. Individual days are colour-coded by their cluster (pale dots) and kernel estimates are contoured (0.05 intervals from 0.05), with northern N_4 in blue, central C_4 in black, mixed M_4 in red, southern S_4 in orange. The crosses mark the NAO/EA values for the cluster centroids, while the squares mark the values for the cluster composites. [Colour figure can be viewed at wileyonlinelibrary.com].

of the EA pattern, respectively, with strong centres of action in the North Atlantic. For the northern jet, the *Z500* pattern is a positive North Atlantic anomaly with a negative anomaly further north (shading, Figure 5(a)). A similar, slightly rotated, *Z500* dipole is present for the AR regime (Figure 6(a)) and the N_4 cluster (Figure 6(e)), and these are in better agreement with each other than they are with the northern jet composite (Figure 5(a)). The eddy-driven jet exhibits a strong southwest–northeast tilt in all cases. For the central jet, the *Z500* pattern is a negative North Atlantic anomaly with a much weaker positive anomaly further south (shading, Figure 5(b)), resembling a diluted version of the patterns for the ZO regime (Figure 6(b)) and C_4 cluster (Figure 6(b)). The strength of the *Z500* anomalies are comparable for the ZO regime and C_4, but the positive anomalies over central Europe are missing in C_4. The eddy-driven jet is strong (large area $> 15\,\mathrm{m\,s^{-1}}$) and tilted for the preferred central jet, the ZO regime, and the C_4 cluster.

None of the preferred jet location composites exhibits positive geopotential anomalies over northern Europe and Scandinavia, as is characteristic of the BL regime (Figure 6(c)). The mixed M_4 cluster does (Figure 6(g)). Furthermore, the eddy-driven jet for the mixed cluster (black contours) is split into two branches, one in the southeastern part of the sector and one over northern Europe, just as the jet for the BL regime. This jet configuration is exemplified by the synoptic situation in Figure 2(c), where a strong anticyclone sits over Scandinavia (identified as a block following the approach of Schwierz *et al.* (2004), section 2.5) and the jet is discontinuous over the North Atlantic.

We now see that European/Scandinavian blocking is not decoupled from the eddy-driven jet, but rather associated with the mixed-jet cluster. Blocking episodes are characterized by persistent anticyclones that can interrupt the mean westerly flow. When such an anticyclone is over Scandinavia, the jet is more likely to be disturbed or split over the North Atlantic sector, as in cluster M_4. The JLI struggles to identify these disturbed jets such that, from the JLI viewpoint, it appears that the jet can occur at any latitude during European/Scandinavian blocking (red line, Figure 4(b)).

We can quantify the distinctive blocking patterns associated with the jet clusters, according to the PV-based blocking index. This shows an enhancement in the blocking frequency of more than 30% over Europe and Scandinavia during mixed cluster days (shading, Figure 7(c)), supporting the results of the weather regime analysis. As in other studies, there is also evidence of enhanced blocking over southwest Europe and offshore of the Iberian peninsula for the northern cluster (Figure 7(a)), while the southern cluster exhibits enhanced blocking frequencies of up to 25% over Greenland (Figure 7(d)). The central cluster (Figure 7(b)) has been referred to as the unperturbed state (e.g. Woollings *et al.*, 2010) and exhibits up to 25% less blocking over the British Isles and northwest Europe. Thus, there is a link between the preferred blocking locations, the eddy-driven jet and the large-scale flow regimes in the North Atlantic (similar to the results of Stan and Straus, 2007, for the North Pacific). These general patterns are also seen in the example synoptic situations presented earlier (Figures 2(a)–(c)), where the blocking anticyclones are found in different places depending on which cluster the day belongs to. For the N_4 day (Figure 2(a)), there is a strong upper-level ridge (red 2 pvu contour) and surface high pressure system (shading) located over the Atlantic. For the S_4 cluster (Figure 2(b)) and M_4 cluster (Figure 2(c)) these features are located over Greenland and Europe/Scandinavia, respectively.

Further corroboration that the jet and weather regimes perspectives are consistent comes from examining how individual days are categorized in each framework. The relative frequencies of the four weather regimes are 23% AR (732 days), 29% ZO (926 days), 26% BL (805 days) and 22% GA (687 days), in good agreement with a similar analysis done using ERA-40 extended winters from 1958 to 2001 (Michel and Rivière, 2011). Within the AR regime, most (70%) days are classified in the N_4 cluster (blue bar, Figure 8(a)), with some days coming from C_4 (black) and M_4 (red), and very few from S_4 (orange). Within the ZO regime (Figure 8(b)), more than half of the days are classified in the C_4 cluster, with the remaining days coming equally from the other three clusters. Within the BL regime (Figure 8(c)) the M_4 cluster dominates (63%), and within the GA regime the S_4 cluster is most frequent (58%). The jet clusters and weather regimes are computed based on slightly different domains and different atmospheric variables, but these results nevertheless indicate that eddy-driven jet variability is closely related to large-scale conditions over Europe.

6. Discussion

The clustering results help clarify the relationship between eddy-driven jet locations and weather regimes, but raise some additional considerations. In this section, we contextualize how the jet clusters are related to the NAO and EA indices, discuss the within-cluster variability, and position the $k = 5$ clustering results (in particular the tilted cluster) within the weather regime framework.

Previous studies showed that the latitude of the eddy-driven jet is connected to the NAO and EA teleconnection patterns (Woollings *et al.*, 2010; Franzke *et al.*, 2011; Davini *et al.*, 2012; Woollings and Blackburn, 2012) – both patterns must be considered, although they are not always sufficient, to describe variations in jet latitude and strength (see also Fyfe and Lorenz, 2005; Monahan and Fyfe, 2006). We examine how the jet clusters are distributed in NAO-EA phase space (Figure 9). The four clusters are not clearly associated with distinct values of the NAO and EA indices, although each cluster tends to reside in a certain quadrant. The southern jet location has been associated with the negative NAO phase (e.g. Woollings *et al.*, 2010; Hannachi *et al.*, 2012); the southern cluster (orange contours and dots) has its centroid in negative NAO space, but includes a considerable number of positive NAO days, and is actually better distinguished by the EA index being mainly positive. A similar conclusion can be drawn from the geopotential anomalies associated with

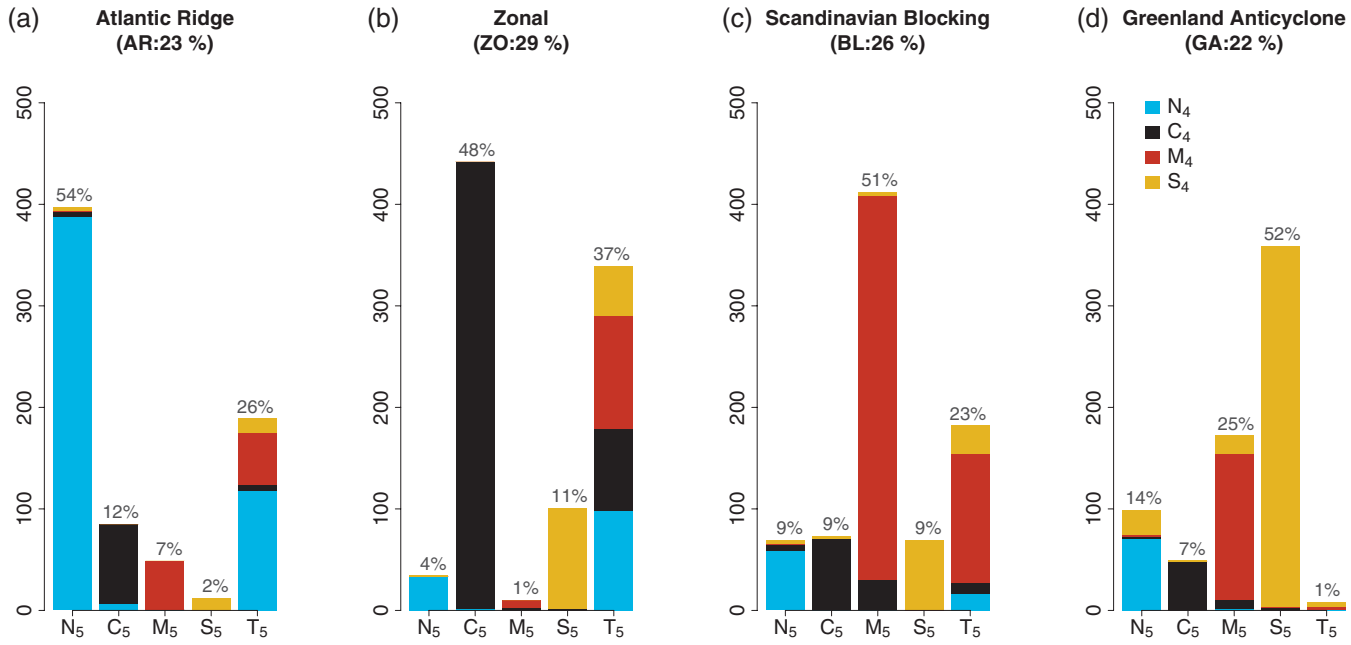

Figure 10. Partitioning of North Atlantic-European weather regimes by jet cluster, similar to Figure 8 but comparing the $k = 4$ and $k = 5$ results, showing results for the four regimes: (a) Atlantic ridge, (b) zonal, (c) Scandinavian blocking, and (d) Greenland anticyclone. Bars indicate the number of days belonging to each $k = 5$ cluster: northern N_5, central C_5, mixed M_5, southern S_5, and tilted T_5. Colours indicate how these days correspond to the $k = 4$ clusters: northern N_4 in blue, central C_4 in black, mixed M_4 in red, and southern S_4 in orange. The occurrence of each weather regime (in %) is shown at the top of each panel. The frequency of each $k = 5$ cluster within the regimes (in %) is shown at the top of the bars, and add up to 100% in each panel. Figure 8 is recovered by stacking segments of the same colour in each panel of this figure. [Colour figure can be viewed at wileyonlinelibrary.com].

S_4 (Figure 5(h)), as the centres of action are offset slightly west of the NAO centres of action. When the NAO and EA are both positive, the jet is mostly in the central cluster. The northern cluster and mixed cluster overlap most in NAO-EA phase space, and both are found mainly when the EA index is negative. The small region where N_4 is distinct from M_4 (negative NAO, negative EA quadrant) is where Woollings *et al.* (2010) observed a sharp transition in the JLI (cf. their Figure 11), suggesting that an ambiguous region in the zonal-mean framework might be better distinguished in a zonally varying framework. The present study confirms that the variability of the eddy-driven jet is complex and cannot be described by a single index. Furthermore, our results do not support a one-to-one correspondence of the ZO (GA) regime with the positive (negative) NAO.

The variability within each cluster exhibits distinct spatial patterns, independent of the choice of k (shading, Figure 3). For example, the highest standard deviations for the C_k clusters are found on the flanks of the jet, suggesting meridional shifting, whereas in the N_k clusters they coincide with the jet maximum, suggesting changes in jet speed (pulsing). Since the eddy-driven jet is maintained by eddy feedbacks (e.g. Hoskins *et al.*, 1983; Lorenz and Hartmann, 2001), these different variability patterns could indicate that different eddy-mean flow interactions dominate each jet configuration. The location of the jet dictates wave breaking patterns in idealized experiments (Rivière, 2009), with more anticyclonic (cyclonic) wave breaking for northern (southern) jets. Jet location has also been found to affect eddy propagation due to spherical geometry effects (Barnes and Hartmann, 2011; Lachmy and Harnik, 2016): because the stationary wavenumber decreases with increasing latitude (due to decreasing beta, the meridional gradient of absolute vorticity (Hoskins and Karoly, 1981)), eddies tend to be reflected rather than to break (cyclonically) on the northern flank of the jet when it is located far to the north. Thus, high-latitude jets should experience less shifting variability and more pulsing variability, as suggested by the within-cluster standard deviation patterns of the N_k clusters (Figure 3). When the jet is far south, the eddy-driven jet can merge with the subtropical jet, concentrating variability on its northern flank (Barnes and Hartmann, 2011), as is seen for the S_k clusters.

Table 3. Pattern correlations Rp as in Table 1, but showing correlations across as well as within $k = 3$, $k = 4$ and $k = 5$ clustering results.

Cluster	N_3 / N_4 / N_5	C_3 / C_4 / C_5	M_3 / M_4 / M_5
N_3	1.00 / 0.99 / 0.96		
N_4	0.99 / 1.00 / 0.99		
C_3		1.00 / 0.93 / 0.93	
C_4		0.93 / 1.00 / 0.93	
M_3			1.00 / 0.99 / 0.97
M_4			0.99 / 1.00 / 0.95
S_4	0.31 / 0.22 / 0.12	0.87 / 0.65 / 0.65	0.58 / 0.51 / 0.48
T_5	0.94 / 0.91 / 0.84	0.77 / 0.87 / 0.86	0.76 / 0.83 / 0.62

The upper part of the table shows Rp between the N_k, C_k and M_k clusters obtained using different k. The lower part of the table shows Rp with the new clusters that emerge with higher k.

While we have focused on the clustering results using $k = 4$ clusters, there is further insight to be gained from the tilted jet that emerges in the $k = 5$ clusters. The tilted cluster mainly occurs in the zonal regime (37% of the time, Figure 10(b), T_5 on the x-axis) but also in the AR (26%) and BL (23%) regimes. Many of the T_5 days were previously classified as N_4 and M_4 (blue and red colours in the T_5 bars), and the composites of these clusters are in fact very similar ($Rp(T_5, N_4) = 0.91$ and $Rp(T_5, M_4) = 0.87$; Table 3). The other $k = 5$ clusters (N_5, C_5, M_5 and S_5) correspond quite well to their $k = 4$ counterparts (stacked bars dominated by one single colour, Figure 10). This suggests that the tilted jet cluster could be a variation of the central jet cluster.

The choice of an appropriate metric (jet clusters, weather regimes, JLI, NAO/EA) to use for characterizing eddy-driven jet variability depends largely on the purpose of the study and the available data. The JLI is eminently useful for its simplicity, and is a good choice when a continuous time series of unique, daily values is desired (e.g. for summarizing changes in the state of the eddy-driven jet over time or under different forcing scenarios or quantitatively comparing the jet state on two days). It can be used over limited time periods and does not require high-resolution data. In interpreting JLI-based results, however, issues like the inability to capture split or tilted jets and sensitivity to orography should be kept in mind. Similarly, the NAO/EA

indices are simple and can be used on limited datasets, but they must be used in combination and even then are not a direct measure of the various jet configurations. In general, the NAO/EA indices and the JLI do not necessarily capture the same jet variability in models as in observations (e.g. Merz *et al.,* 2015; Masato *et al.,* 2016), making it difficult to use them as metrics for model comparisons. Weather regimes and jet clusters provide the most complete picture of the variability because they capture the two-dimensional spatial patterns. These two complementary metrics should thus be preferred, for example, when studying the dynamics of weather extremes. They could also provide a more robust framework for evaluating model biases. However, to correctly represent the jet clusters and weather regimes requires higher spatial resolution than is afforded by current climate models (Dawson *et al.,* 2012) as well as a large sample size (i.e. a long enough time series to capture the full variability). Ideally, one would use a combination of metrics rather than relying on a single one in order to ensure a more accurate representation of the eddy-driven jet variability.

7. Concluding remarks

This study links two different perspectives on wintertime variability in the North Atlantic sector: the JLI framework that comprises three preferred eddy-driven jet locations (Woollings *et al.,* 2010), and the weather regime framework that comprises four North Atlantic–European weather regimes (e.g. Vautard, 1990; Michelangeli *et al.,* 1995). A *k*-mean clustering algorithm is used to characterize the variability of the eddy-driven jet, as defined by the two-dimensional low-level wind field. This analysis allows us to extend the zonal-mean picture provided by the JLI, and thus to account for more complex jet configurations such as tilted or split jets. The main conclusions are:

1. In addition to the three preferred eddy-driven jet stream locations (southern/central/northern), a new jet configuration (the mixed cluster *M*) is found in the North Atlantic. The mixed cluster represents a split or strongly tilted jet (Figure 6(g)), and is not merely a transition state (Table 2). In the zonal mean perspective, it exhibits a JLI over a range of latitudes, with a slight preference for the northern and southern locations (Figure 4(b)).
2. With the clustering results, we can now reconcile eddy-driven jet variability with the four classical weather regimes. The four North Atlantic jet clusters are linked to the four North Atlantic–European weather regimes and their associated blocking patterns (Figures 6 and 7). During European/Scandinavian blocking, the jet is mainly in the newly identified mixed cluster (Figure 8).

There remains more to investigate on the mechanisms responsible for the persistence of the four jet clusters, what drives their transitions, and whether preferred transition paths exist. There have been studies on the transitions between preferred jet locations (Hannachi *et al.,* 2012) and the role of wave breaking in these transitions (Franzke *et al.,* 2011). It is the aim of future work to include the mixed-jet configuration in similar analyses, and further bridge to weather regime transitions (Michel and Rivière, 2011). The role of eddy–mean flow interactions in determining the within-cluster variability will also be explored.

Acknowledgements

We thank Clio Michel, Lukas Papritz, Stephan Pfahl and Julian Quinting for fruitful discussions. We acknowledge Julian Quinting for providing the k-means clustering code in NCL. This work was supported by the Research Council of Norway project jetSTREAM (231716). CMG acknowledges funding from the Swiss National Science Foundation (SNSF) via grant PZ00P2_148177/1 and a Bjerknes Visiting Fellowship from the Bjerknes Centre for Climate Research for stimulating this collaboration. We are grateful to the reviewers for their constructive comments.

References

Athanasiadis PJ, Wallace JM, Wettstein JJ. 2010. Patterns of wintertime jet stream variability and their relation to the storm tracks. *J. Atmos. Sci.* **67**: 1361–1381.

Barnes EA, Hartmann DL. 2011. Rossby wave scales, propagation, and the variability of eddy-driven jets. *J. Atmos. Sci.* **68**: 2893–2908.

Barnes EA, Hartmann DL, Frierson DMW, Kidston J. 2010. Effect of latitude on the persistence of eddy-driven jets. *Geophys. Res. Lett.* **37**: L11804. https://doi.org/10.1029/2010GL043199.

Baur F, Hess P, Nagel H. 1944. *Kalender der Grosswetterlagen Europas 1881–1939*. DWD: Bad Homburg, Germany.

Benedict JJ, Lee S, Feldstein SB. 2004. Synoptic view of the North Atlantic oscillation. *J. Atmos. Sci.* **61**: 121–144.

Cassou C. 2008. Intraseasonal interaction between the Madden–Julian Oscillation and the North Atlantic Oscillation. *Nature* **455**: 523–527. https://doi.org/10.1038/nature07286.

Cattiaux J, Vautard R, Cassou C, Yiou P, Masson-Delmotte V, Codron F. 2010. Winter 2010 in Europe: A cold extreme in a warming climate. *Geophys. Res. Lett.* **37**: L20704. https://doi.org/10.1029/2010GL044613.

CDO. 2015. *Climate Data Operators*. Hamburg, Germany http://www.mpimet.mpg.de/cdo (accessed 8 September 2017): Max-Planck Institut.

Cheng X, Wallace JM. 1993. Cluster analysis of the northern hemisphere wintertime 500-hPa height field: Spatial patterns. *J. Atmos. Sci.* **50**: 2674–2696.

Davini P, Cagnazzo C, Neale R, Tribbia J. 2012. Coupling between Greenland blocking and the North Atlantic Oscillation pattern. *Geophys. Res. Lett.* **39**: L14701. https://doi.org/10.1029/2012GL052315.

Davini P, Cagnazzo C, Fogli PG, Manzini E, Gualdi S, Navarra A. 2014. European blocking and Atlantic jet stream variability in the NCEP/NCAR reanalysis and the CMCC-CMS climate model. *Clim. Dyn.* **43**: 71–85. https://doi.org/10.1007/s00382-013-1873-y.

Dawson A, Palmer TN, Corti S. 2012. Simulating regime structures in weather and climate prediction models. *Geophys. Res. Lett.* **39**: L21805. https://doi.org/10.1029/2012GL053284.

Dee DP, Uppala SM, Simmons AJ, Berrisford P, Poli P, Kobayashi S, Andrae U, Balmaseda MA, Balsamo G, Bauer P, Bechtold P, Beljaars ACM, van de Berg L, Bidlot J, Bormann N, Delsol C, Dragani R, Fuentes M, Geer AJ, Haimberger L, Healy SB, Hersbach H, Hólm EV, Isaksen L, Kållberg P, Köhler M, Matricardi M, McNally AP, Monge-Sanz BM, Morcrette J-J, Park BK, Peubey C, de Rosnay P, Tavolato C, Thépaut J-N, Vitart F. 2011. The ERA-Interim reanalysis: Configuration and performance of the data assimilation system. *Q. J. R. Meteorol. Soc.* **137**: 553–597. https://doi.org/10.1002/qj.828.

Eichelberger SJ, Hartmann DL. 2007. Zonal jet structure and the leading mode of variability. *J. Clim.* **20**: 5149–5163.

Ferranti L, Corti S, Janousek M. 2015. Flow-dependent verification of the ECMWF ensemble over the Euro-Atlantic sector. *Q. J. R. Meteorol. Soc.* **141**: 916–924.

Frame THA, Ambaum MHP, Gray SL, Methven J. 2011. Ensemble prediction of transitions of the North Atlantic eddy-driven jet. *Q. J. R. Meteorol. Soc.* **137**: 1288–1297.

Franzke C, Woollings T, Martius O. 2011. Persistent circulation regimes and preferred regime transitions in the North Atlantic. *J. Atmos. Sci.* **68**: 2809–2825.

Fyfe JC, Lorenz DJ. 2005. Characterizing midlatitude jet variability: Lessons from a simple GCM. *J. Clim.* **18**: 3400–3404.

Grams CM, Beerli R, Pfenninger S, Staffell I, Wernli H. 2017. Balancing Europe's wind-power output through spatial deployment informed by weather regimes. *Nature Clim. Change* **7**: 557–562. https://doi.org/10.1038/nclimate3338.

Hannachi A, Woollings T, Fraedrich K. 2012. The North Atlantic jet stream: A look at preferred position, paths and transitions. *Q. J. R. Meteorol. Soc.* **138**: 862–877.

Hannachi A, Straus DM, Franzke CLE, Corti S, Woollings T. 2017. Low-frequency nonlinearity and regime behavior in the Northern Hemisphere extratropical atmosphere. *Rev. Geophys.* **55**: 199–234.

Harnik N, Galanti E, Martius O, Adam O. 2014. The anomalous merging of the African and North Atlantic jet streams during the Northern Hemisphere winter of 2010. *J. Clim.* **27**: 7319–7334.

Held IM. 1975. Momentum transport by quasi-geostrophic eddies. *J. Atmos. Sci.* **32**: 1494–1497.

Held IM, Hou AY. 1980. Nonlinear axially symmetric circulations in a nearly inviscid atmosphere. *J. Atmos. Sci.* **37**: 515–533.

Hoskins BJ, Karoly DJ. 1981. The steady linear response of a spherical atmosphere to thermal and orographic forcing. *J. Atmos. Sci.* **38**: 1179–1196.

Hoskins BJ, James IN, White GH. 1983. The shape, propagation and mean-flow interaction of large-scale weather systems. *J. Atmos. Sci.* **40**: 1595–1612.

Hurrell JW. 1995. Decadal trends in the North Atlantic Oscillation: Regional temperatures and precipitation. *Science* **269**: 676–679.

Kimoto M, Ghil M. 1993. Multiple flow regime in the Northern Hemisphere winter. *Part I: Methodology and Hemispheric regimes. J. Atmos. Sci.* **50**: 2625–2643.

Koch P, Wernli H, Davies HC. 2006. An event-based jet-stream climatology and typology. *Int. J. Climatol.* **26**: 283–301.

Lachmy O, Harnik N. 2016. Full access wave and jet maintenance in different flow regimes. *J. Atmos. Sci.* **73**: 2465–2484.

Lee S, Kim HK. 2003. The dynamical relationship between subtropical and eddy-driven jets. *J. Atmos. Sci.* **60**: 1490–1503.

Li C, Wettstein JJ. 2012. Thermally driven and eddy-driven jet variability in reanalysis. *J. Clim.* **25**: 1587–1596.

Limbach S, Schömer E, Wernli H. 2012. Detection, tracking and event localization of jet stream features in 4D atmospheric data. *Geosci. Model Dev.* **5**: 457–470. https://doi.org/10.5194/gmd-5-457-2012.

Lorenz DJ, Hartmann DL. 2001. Eddy-zonal flow feedback in the Southern Hemisphere. *J. Atmos. Sci.* **58**: 3312–3327.

Lorenz DJ, Hartmann DL. 2003. Eddy-zonal flow feedback in the Northern Hemisphere winter. *J. Clim.* **16**: 1212–1227.

Luo D, Yao Y, Feldstein SB. 2014. Regime transition of the North Atlantic Oscillation and the extreme cold event over Europe in January–February 2012. *Mon. Weather Rev.* **142**: 4735–4757.

Masato G, Woollings T, Williams K, Hoskins BJ, Lee RW. 2016. A regime analysis of Atlantic winter jet variability applied to evaluate HadGEM3-GC2. *Q. J. R. Meteorol. Soc.* **142**: 3162–3170.

Merz N, Raible CC, Woollings T. 2015. North Atlantic eddy-driven jet in interglacial and glacial winter climates. *J. Clim.* **28**: 3977–3997.

Messori G, Caballero R. 2015. On double Rossby wave breaking in the North Atlantic. *J. Geophys. Res. Atmos.* **120**: 11129–11150. https://doi.org/10.1002/2015JD023854.

Michel C, Rivière G. 2011. The link between Rossby wave breakings and weather regime transitions. *J. Atmos. Sci.* **68**: 1730–1748.

Michelangeli P, Vautard R, Legras B. 1995. Weather regimes: Recurrence and quasi stationarity. *J. Atmos. Sci.* **52**: 1237–1256.

Molteni F, Tibaldi S, Palmer TN. 1990. Regimes in the wintertime circulation over northern extratropics. I: Observational evidence. *Q. J. R. Meteorol. Soc.* **116**: 31–67.

Monahan AH, Fyfe JC. 2006. On the nature of zonal jet EOFs. *J. Clim.* **19**: 6409–6424.

Namias J. 1953. *Thirty-day Forecasting – A Review of a Ten-year Experiment*. *Meteorological Monographs*, Vol. **2**. Boston, MA: American Meterorological Society.

Ouzeau G, Cattiaux J, Douville H, Ribes A, Saint-Martin D. 2011. European cold winter 2009–2010: How unusual in the instrumental record and how reproducible in the ARPEGE--Climat model? *Geophys. Res. Lett.* **38**: L11706. https://doi.org/10.1029/2011GL047667.

Panetta RL. 1993. Zonal jets in wide baroclinically unstable regions: Persistence and scale selection. *J. Atmos. Sci.* **50**: 2073–2106.

Pfahl S, Schwierz C, Croci-Maspoli M, Grams CM, Wernli H. 2015. Importance of latent heat release in ascending air streams for atmospheric blocking. *Nat. Geosci.* **8**: 610–614.

Reinhold BB, Pierrehumbert RT. 1982. Dynamics of weather regimes: Quasi-stationary waves and blocking. *Mon. Weather Rev.* **110**: 1105–1145.

Rhines PB. 1975. Waves and turbulence on a β-plane. *J. Fluid Mech.* **69**: 417–443.

Rivière G. 2009. Effect of latitudinal variations in low-level baroclinicity on eddy life cycles and upper-tropospheric wave-breaking processes. *J. Atmos. Sci.* **66**: 1569–1592.

Rivière G, Orlanski I. 2007. Characteristics of the Atlantic storm-track eddy activity and its relation with the North Atlantic Oscillation. *J. Atmos. Sci.* **64**: 241–266.

Santos JA, Woollings T, Pinto JG. 2013. Are the winters 2010 and 2012 archetypes exhibiting extreme opposite behavior of the North Atlantic jet stream? *Mon. Weather Rev.* **141**: 3626–3640.

Schiemann R, Lüti D, Schär C. 2009. Seasonality and interannual variability of the westerly jet in the Tibetan plateau region. *J. Clim.* **22**: 2940–2957.

Schneider EK. 1977. Axially symmetric steady-state models of the basic state for instability and climate studies. Part II. Nonlinear circulations. *J. Atmos. Sci.* **34**: 280–296.

Schwierz C, Croci-Maspoli M, Davies HC. 2004. Perspicacious indicators of atmospheric blocking. *Geophys. Res. Lett.* **31**: L06125. https://doi.org/10.1029/2003GL019341.

Spensberger C, Spengler T, Li C. 2017. Upper tropospheric jet axis detection and application to the boreal winter 2013/2014. *Mon. Weather Rev.* **145**: 2363–2374. https://doi.org/10.1175/MWR-D-16-0467.1.

Stan C, Straus DM. 2007. Is blocking a circulation regime? *Mon. Weather Rev.* **135**: 2406–2413.

Thompson DWJ, Lee S, Baldwin MP. 2003. Atmospheric processes governing the Northern Hemisphere Annular Mode/North Atlantic Oscillation. In *The North Atlantic Oscillation: Climatic Significance and Environmental Impact*, Hurrell JW, Kushnir Y, Ottersen G, Visbeck M. (eds.). American Geophysical Union: Washington, DC. https://doi.org/10.1029/134GM05.

Thorncroft C, Hoskins BJ, McIntyre ME. 1993. Two paradigms of baroclinic wave life cycle behaviour. *Q. J. R. Meteorol. Soc.* **119**: 17–55.

Vallis GK, Gerber EP. 2008. Local and hemispheric dynamics of the North Atlantic Oscillation, annular patterns and the zonal index. *Dyn. Atmos. Oceans* **44**: 184–212.

Vautard R. 1990. Multiple weather regimes over the North Atlantic: Analysis of precursors and successors. *Mon. Weather Rev.* **118**: 2056–2081.

Wallace JM, Gutzler DS. 1981. Teleconnections in the geopotential height field during the Northern Hemisphere winter. *Mon. Weather Rev.* **109**: 784–812.

Wanner H, Brönnimann S, Casty C, Gyalistras D, Luterbacher J, Schmutz C, Stephenson D, Xoplaki E. 2001. North Atlantic Oscillation – concepts and studies. *Surv. Geophys.* **22**: 321–381.

Woollings T, Blackburn M. 2012. The North Atlantic jet stream under climate change and its relation to the NAO and EA patterns. *J. Clim.* **25**: 886–902.

Woollings T, Hannachi A, Hoskins B. 2010. Variability of the North Atlantic eddy-driven jet stream. *Q. J. R. Meteorol. Soc.* **136**: 856–868.